Removal of antimonite (III) from wastewater using sodium-alginate-modified Fe-attapulgite with sodium alginate beads

Aixia Zhou, Jinsheng Wang*

College of Water sciences, Beijing Normal University, Beijing, 100088, China, Tel. +86 13811500321;
emails: wangjs@bnu.edu.cn (J.S. Wang), zhouaixia2010@sina.com (A.X. Zhou)

ABSTRACT

Antimony (Sb) is a potentially carcinogenic metalloid and is listed as a high priority pollutant by the World Health Organization. We used $FeCl_3$-modified attapulgite (ATP) incorporating sodium alginate (SA) to synthesize an Fe-ATP bead for Sb(III) removal from the aquatic environment. The parameters of the adsorption process, including pH, temperature, and initial contaminant loading, were systematically optimized. The results indicated that the optimum solution pH range was 1.0–11.0, and the adsorption capacity was up to 39.24 mg g^{-1}. The value of $\Delta H°$ (2.973 kJ mol^{-1}) and $\Delta G°$ (−2.6668 kJ mol^{-1} (303.15 K), −2.8558 kJ mol^{-1} (313.15 K), −3.0364 kJ mol^{-1} (323.15 K)) showed that the Sb(III) adsorption onto Fe-ATP beads was a spontaneous endothermic process and the adsorption efficiency increases with temperature. The adsorption generally reached equilibrium after 20 min. The Sb(III) adsorption efficiency onto Fe-ATP beads remained greater than 80% after 5 regeneration cycles. In view of the broad applicable pH and high adsorption capacity, Fe-ATP bead is a potential adsorbent for Sb(III) recovered from polluted water.

Keywords: Adsorption; Sb(III); Fe-modified attapulgite (ATP); Sodium alginate (SA)

1. Introduction

For decades, antimony (Sb) contamination in aquatic environments has caused global concern [1]. Sb is used in various industrial products, for example, brake linings, battery grids, semiconductors, flame retardants, and as paint pigment components [2–6]. The most common forms of Sb in the aquatic environment are inorganic forms. The trivalent form of Sb is ten times more harmful than the pentavalent forms [2].

The Sb concentration ranged from 0.03 to 0.07 µg L^{-1} in surface water samples from 11 different countries and regions [3]. The Sb(III) concentration in the Yangtze River of China was from 0.029 to 0.736 µg L^{-1} [4]. Sb has been detected in the groundwater of many countries and Sb pollution in groundwater has become a cause for concern [1]. Sb(III) pollution results in adverse impacts on the local ecosystem, including drinking water, food, and human health [7,8]. Therefore, effective methods of Sb (Sb(III)) removal from contaminated wastewater or groundwater are important for improving the aquatic environment and protecting human health.

The adsorption is an efficient technique for Sb(III) removal from the aquatic environment because of its low-cost, simple operation, and regeneration. Among the most important aspects of the adsorption technique is the choice of adsorbents [5]. Numerous materials as Sb(III) adsorbents have been researched, including commercial activated carbons [6], activated alumina [9], ion exchange resins [10], clay minerals [11,12], bio-materials [13,14], sand [15], and even some wastes [7]. However, these research studies have focused more on stimulated water in the laboratory. Because of their high cost and complexity in manufacturing, as well as due to extreme environmental conditions, it has been

* Corresponding author.

difficult to apply the adsorbents for the treatment of natural waters. Thus, there anis urgent need to find adsorbents that is more applicable to the complex environment. Because NaAlg has many advantages including renewability, abundant sources, nontoxicity, water-solubility, biodegradability, and biocompatibility, it has been used in the decontamination of wastewater fields. Alginate-based Pal foams have been applied as efficient adsorbents for heavy metal adsorption from wastewater with noticeable results [8]. Engineered NaAlg-based beads also have been utilized to adsorb toxic metal ions and cationic dyes [16]. However, research regarding the use of sodium-alginate-attapulgite to adsorb Sb(III) ions is rare.

In this study, Fe-attapulgite (ATP) beads were developed to remove Sb(III) ions from solution. The influence of pH, contact time, and initial concentration on adsorption was investigated. The adsorption mechanism for Sb(III) onto the Fe-ATP beads is proposed. Thus, these results may promote the development of decontamination technologies for Sb(III)-contaminated water.

2. Experimental

2.1. Materials

Attapulgite was obtained from Xuyi City, Jiangsu Province, China. Reagent grade anhydrous ferric chloride ($FeCl_3$), sodium alginate (SA), Sb potassium tartrate ($KSbC_4H_4O_7 \cdot 1/2H_2O$), and the other reagents were purchased from the Sinopharm Chemical Reagent Co. Ltd., (Shanghai, China). $KSbC_4H_4O_7 \cdot 1/2H_2O$ was dissolved in deionized water to prepare the Sb(III) stock solution.

The Fe-ATP beads were produced according to the procedure of Zhou et al. [5]. ATP was sieved to 200 British Standard Sieve (BSS) mesh. Then, ATP powder was added to 2.0 mol L^{-1} $FeCl_3$ solution (prepared using dilute hydrochloric acid) with a ratio (v/w) of 5:1 ($FeCl_3$/ATP) to exchange the interlayer cations with Fe^{3+}. The mixture was stirred for 90 min under magnetic stirring (H01-1B, Shanghai Mei Yingpu Instrument Manufacturing Co. Ltd, Shanghai, China) and dispersed in an ultrasonic bath (KQ-250DB, Kun Shan Ultrasonic Instruments Co. Ltd, Kunshan, China) for 1.0 h at 308 K. The precipitate was separated by centrifuging at 3,300 r min^{-1} for 15 min (Biofuge primo R, Thermo Sorvall, Shanghai, China) and repeatedly washed to remove the water-soluble particles. It was then filtered. The Fe-ATP powder was aged for 2.0 h at 353 K and then dried, crushed, and sieved to the particle size of a 100 mesh screen. The Fe-ATP powder was mixed with sodium alga acid and dropped into a calcium chloride solution at a constant velocity to form the beads. The beads were dried for 2.0 h at 383 K and stored in an airtight container until further use.

2.2. Sb(III) adsorption and desorption experiments

Sb(III) adsorption by Fe-ATP beads was investigated using batch experiments under controlled experimental conditions (pH, initial concentration, temperature, and contact time). Fe-ATP beads (0.05 g) were placed in a polyethylene bottle (100 mL) with 50 mL of Sb(III) solution (1.0–100.0 mg L^{-1}) and at a pH value of 1.0–13.0. The batch experiments were conducted using an automatic shaker agitated at a speed of 200 rpm at 303.15 K for the required time. An HCl or NaOH solution was used to adjust the pH values of the solution. The effect of temperature was investigated by adjusting temperature values within the range of 303.15–323.15 K using a thermostat. All experiments were repeated in triplicate to determine the accuracy of the procedure. Pure SA beads had no adsorption function on the Sb(III) ions and the adsorption data did not show in the results.

The Sb(III) concentration of the solution was measured using inductively coupled plasma mass spectrometry. The adsorption rate (Adsorption, %) and adsorption capacity (q_t, mg g^{-1}) were calculated using Eqs. (1) and (2), respectively, as follows:

$$q_t = \frac{V \times (C_0 - C_t)}{m} \tag{1}$$

$$\text{Adsorption}(\%) = \frac{(C_0 - C_t)}{C_0} \times 100\% \tag{2}$$

where C_0 is the initial concentration, C_t (mg L^{-1}) is the residual concentration of Sb(III), m(g) is the mass of the adsorbents, and V(L) is the volume of the adsorption system.

Approximately 10.0 g of Fe-ATP beads after adsorption with Sb(III) ions was placed in a conical flask with 50.0 mL of 1.0 mol L^{-1} HCl solution. The de-sorption experiments were conducted at a constant stirring speed for 2.0 h. Then, the Fe-ATP beads were dried at 105°C to a constant weight.

A natural water sample was obtained from surface water and the Sb(III) ion concentration was approximately 0.5 μg L^{-1}. The experimental procedure followed that of the aforementioned experiments.

2.3. Analytical methods

Original ATP and Fe-ATP powder were determined using transmission electron microscopy (TEM; Tecnai G2 20, FEI Company, Hillsboro, USA). Scanning electron microscopy (SEM; Hitachi S-4800/EX-350, Suzhou, China) was utilized to characterize the surface of the Fe-ATP beads. The functional groups on the surface of the Fe-ATP beads were identified using Fourier-transform infrared spectroscopy (FTIR; Nexus 670, Nicolet, USA).

3. Results and discussion

3.1. Characterization of Fe-ATP

The nano-structures of the Fe-ATP powder and beads were observed (Fig. 1). Some rod structures resembling rod fibers were densely overlapped. It was clear that the laden Fe^{3+} ions were on the active sites of the Fe-ATP bead surface. Fig. 1c shows the morphologies of the Fe-ATP beads. The diameter of the Fe-ATP beads was approximately 1.5–2.0 cm.

Fig. 2 shows the FTIR spectra of SA, Fe-ATP, and Fe-ATP beads. As shown in Fig. 2a, 1,579 cm^{-1} was the stretching vibration of the carboxyl group. As shown in Figs. 2b and c, the band at 3,553 cm^{-1} was attributed to the vibrations
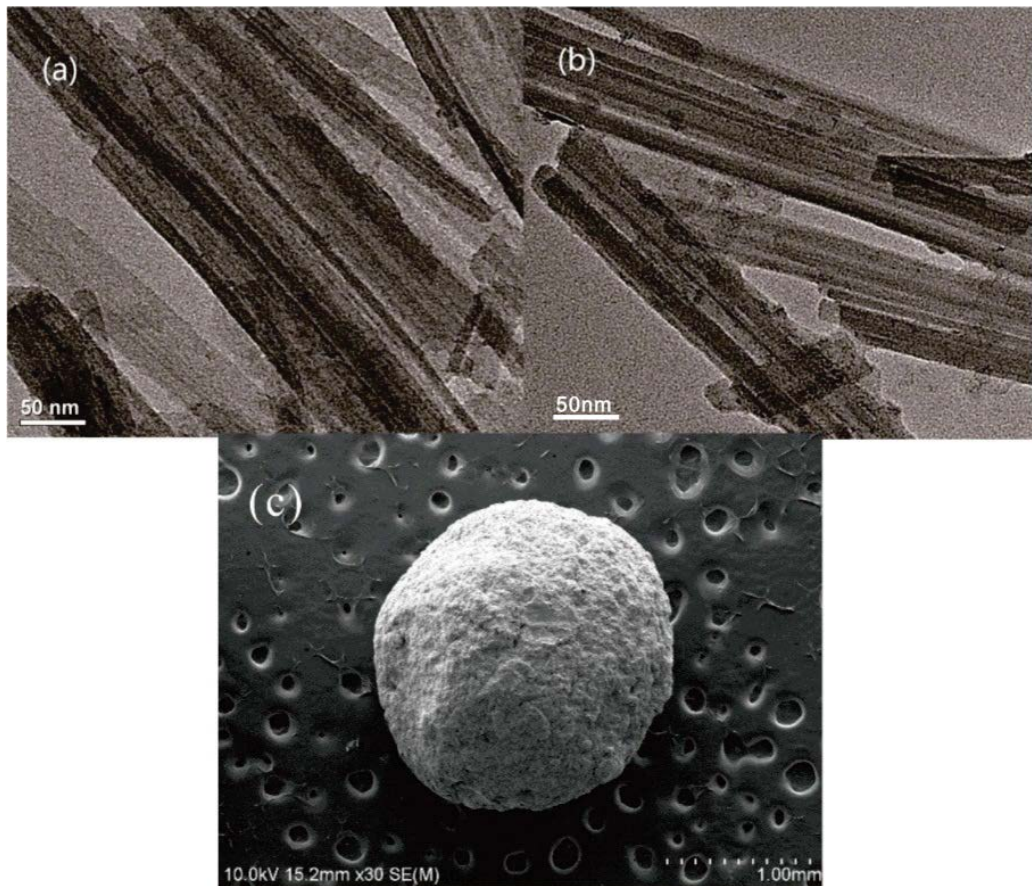
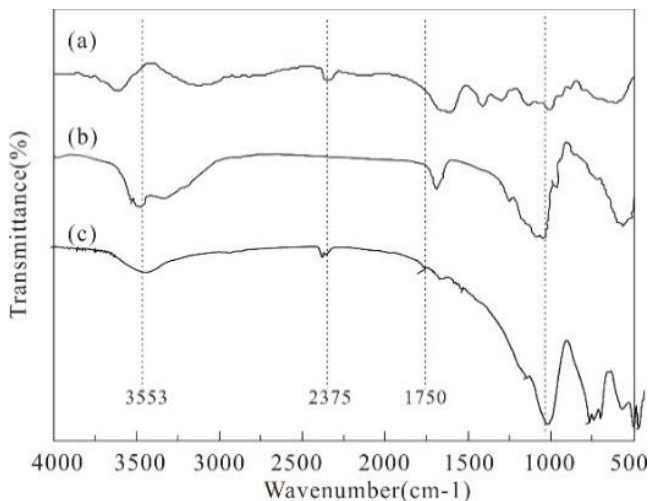Fig. 1. (a,b) TEM results of Fe-ATP powder, and (c) SEM results of Fe-ATP beads.

Fig. 2. FTIR results of (a)SA, (b) Fe-ATP, and (c) Fe-ATP beads.

of hydroxyl groups M–OH (M = Al_2, Al–Mg, Al–Fe^{3+}, Mg and Fe^{3+}) [17–19]. The peak at 2,350 cm^{-1} was a result of the NH_4^- vibration, indicating that the SA had combined with Fe-ATP.

The characteristic peak of Si-O was split into two peaks at 1,031 cm^{-1} and 981 cm^{-1}, respectively, illustrating that there were two connection modes of Si–O in the ATP [20]. The specific adsorption peaks of ATP were 510 and 476 cm^{-1}. The band at 880 cm^{-1} was the vibrational mode of Al–Fe–OH [21]. These data were fundamental in confirming the ATP structure. The Fe-ATP bead maintained the fundamental ATP structure.

3.2. Adsorption of Sb(III) onto Fe-ATP beads

3.2.1. Contact time

The adsorption efficiency of Sb(III) ions onto the Fe-ATP beads increased with contact time (Fig. 3a). Equilibrium was reached after approximately 20 min. A total of 80.7% of the Sb(III) ions was removed from solution after only 10 min, and the adsorption efficiency reached 92.50% after 30 min. The high speed of the adsorption process showed that the Sb(III) ions may be mainly adsorbed on the surface of the Fe-ATP beads. After 30 min, because the adsorption sites were occupied by Sb(III) ions, the adsorption tended to equilibrium and the adsorption rate decreased.

3.2.2. pH

pH is an important parameter that affects the existential state of metal ions in a water solution and the binding sites of metal ions on adsorbent beads [22]. According to the
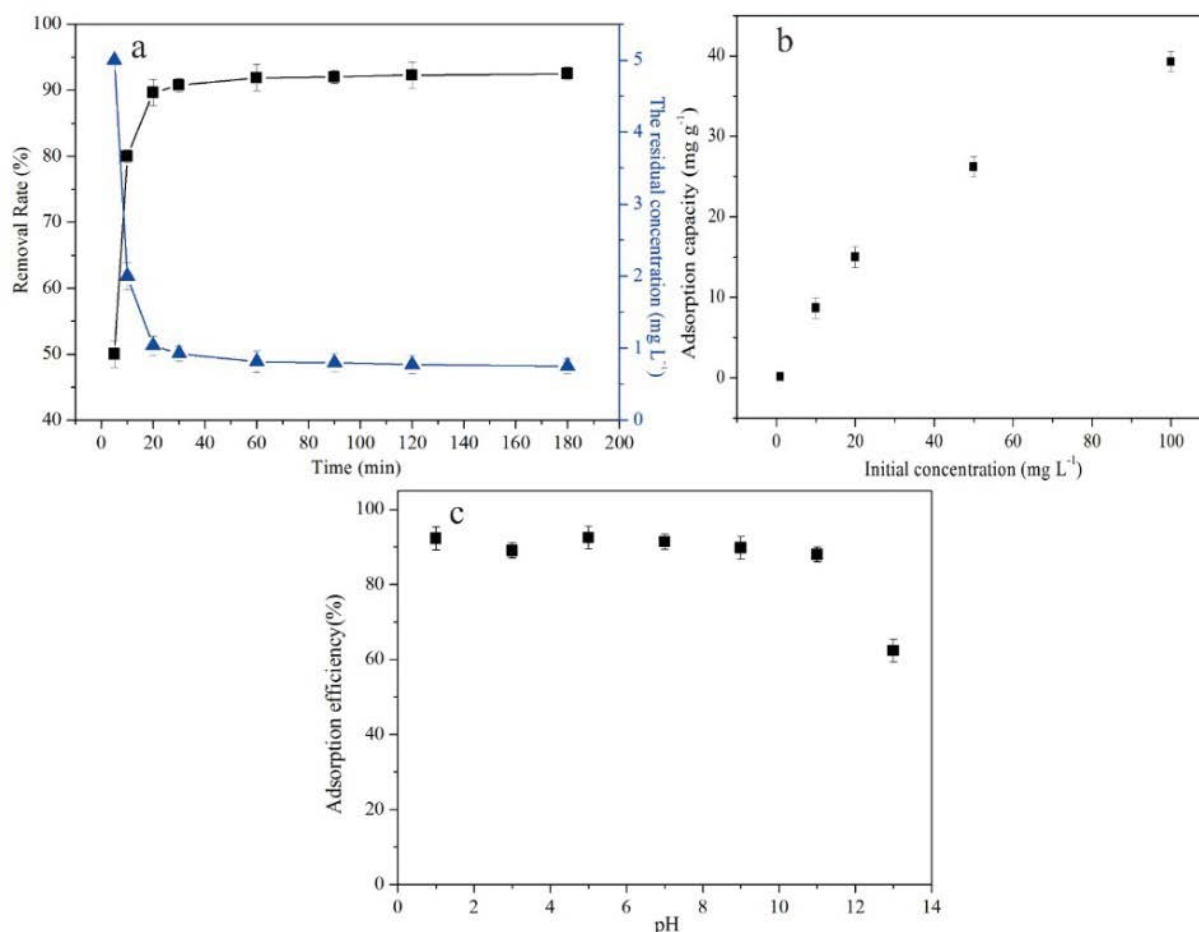
Fig. 3. Influence of environmental factors on Sb(III) ion adsorption onto Fe-ATP beads (a) Time (Initial Sb(III) ion concentration was 100 mg L^{-1}, (b) Initial concentration, and (c) pH.

literature [23,24], at pH 2–11, the principal species of Sb(III) was Sb(OH)$_3$. Sb(OH)$_2^+$ is predominant below pH 1.4 and Sb(OH)$_4^-$ occurs when the pH is above 11.8.

The influence of pH on Sb(III) ion adsorption onto Fe-ATP beads was investigated within a range of 1.0 to 13.0 (as shown in Fig. 3c). The adsorption efficiency of Sb(III) ions onto the Fe-ATP beads was high at pH 1.0–11.0. Because of the buffer function of SA, the influence of pH on Sb(III) ion adsorption onto the Fe-ATP beads was weak. This result also implies that the Sb(III) ion adsorption by Fe-ATP beads could adapt to a broad pH range in the environment.

3.2.3. Initial concentration of Sb(III) ions

Because of the driving mass transfer force, the adsorption capacity remarkably increased with the increase in the Sb(III) ion initial concentration. The maximum adsorption capacity of the Sb(III) ions onto the adsorbent was 39.24 mg g^{-1} when the initial concentration was 100 mg L^{-1}. The Sb(III) ion adsorption capacity on different sorbents in the literature (Table 1) was compared to that of the Fe-ATP beads obtained in this research. Although a direct comparison to other sorbents was difficult because of the various experimental conditions, the results in section 3.2.2 showed that the Sb(III) ion adsorption onto the Fe-ATP beads was possible within

a broad pH range of 1.0–11.0. Therefore, the Fe-ATP beads were more applicable to an actual wastewater environment than the other sorbents in the literature.

3.2.4. Adsorption kinetics

The process of metal ions adsorbing on a solid adsorbent has been described by many models [22]. To evaluate the Sb(III) ion adsorption onto the Fe-ATP beads, pseudo-first-order, pseudo-second-order, intra-particle diffusion kinetic, and Elovich models were used to fit the adsorption process. The linear forms of these models are provided in Eqs. (3)–(6):

$$\ln\left(q_e - q_t\right) = \ln q_e - k_1 t \tag{3}$$

$$\frac{t}{q_t} = \frac{1}{k_2 q_e^2} + \frac{t}{q_e} \tag{4}$$

$$q_t = \left(\frac{1}{\beta}\right)\ln\left(\alpha\beta\right) + \left(\frac{1}{\beta}\right)\ln t \tag{5}$$

$$q_t = k_{pi} t^{1/2} + C_{pi} \tag{6}$$

Table 1
Sb(III) ion adsorption capacity of other adsorbents

Sorbents	Capacity (mg g⁻¹)	Experimental conditions				
		Contact time (h)	pH range	Dosage (g L⁻¹)	Temperature (°C)	References
Modified perlite	76.50	1	4	4	20	[22]
Bentonite	0.37	24	6	25	25	[11]
Diatomite	35.20	0.5	6	4	20	[12]
FeCl$_3$-modifed Sepiolite	21.63	1.5	6.8	2	35	[13]
Chitosan-modified pumice	88.90	1.5	4–5	20	20	[14]
Carbon nanotubes	140.85	3	7	2.5	–	[25]
Hydrochars and pyrochars	11.70	24	6	–	30	[17]
Carbon nanofibers	70.83	1.5	7	1	25	[18]
Ce-doped Fe$_3$O$_4$	43.55	12	7	0.2	25	[19]
FeO(OH)–clinoptilolite tuff	18.58	–	2.6	–	23	[26]
Orange waste	125.90	24	2.5–7.5	1.67	30	[22]
Sodium montmorillonite	38.9	2	–	50	120	[23]
Graphene	7.50	4	11	0.4	30	[24]
Fe-ATP bead	39.24	0.5	1–11	1	30	This study

where q_t is the amount of Sb(III) ions adsorbed at t time (min) and q_e is the amount of Sb(III) ions at equilibrium. k_1 (min⁻¹) is the pseudo-first-order rate constant of the equation, k_2 (g mg⁻¹ min⁻¹) is the second-order rate constant, and k_{pi} (mg g⁻¹ h⁻⁰·⁵) is the rate constant for the intra-particle transport. C_{pi} is the adsorption constant. α (mg g⁻¹ min⁻¹) is the initial adsorption rate of the Elovich equation and β is the extent of the chemisorption surface coverage [11].

The adsorption mechanism of Sb(III) ions onto the Fe-ATP beads can be investigated via adsorption kinetics [12]. The fitted results of four kinetic models for the aforementioned equations are shown in Fig. 4. The fitted parameters were calculated from the linear equation as shown in Table 2. Because the r^2 value of the pseudo-second-order model (0.9996) was greater than that of the other three models, the adsorption process was better described using the pseudo-second-order model rather than the other three kinetic models. The theoretical q_e and actual q_e (9.250 mg g⁻¹) were accordant with each other. Thus, chemisorption could be deemed to be the main mechanism and Sb(III) ions may be attached onto the active sites of the Fe-ATP beads [13].

3.2.5. Adsorption Isotherm

The Sb(III) adsorption on Fe-ATP beads was described using three isotherm models: the Langmuir [14], Freundlich [30] and Dubinin–Radushkevich isotherm models [25]. The feasibility of the isotherm models to show the Sb(III) adsorption on the Fe-ATP beads was estimated according to the r^2 values.

The Freundlich, Langmuir, and Dubinin–Radushkevich equations are shown in Eqs. (7)–(9), respectively, to describe the adsorption isotherms:

$$\frac{C_e}{q_e} = \frac{1}{q_0 b} + \frac{C_e}{q_0} \tag{7}$$

$$\log q_e = \log K_f + \left(\frac{1}{n}\right)\log C_e \tag{8}$$

$$\varepsilon = RT \ln\left(1 + \frac{1}{C_{eq}}\right) \tag{9}$$

where C_e is the Sb(III) ion concentration at equilibrium (mg L⁻¹), q_e is the Sb(III) adsorption capacity at equilibrium (mg g⁻¹), b is the Langmuir constant (L mg⁻¹), and q_0 is the saturated monolayer adsorption capacity (mg g⁻¹). K_f is the Freundlich constant [(mg g⁻¹) (L mg⁻¹)⁻¹ᐟⁿ]. T is the temperature (K), R is 8.314 J mol⁻¹ K⁻¹, and C_{eq} is the Sb(III) ion concentration in the solution at equilibrium (mol L⁻¹).

Table 2
Kinetic model constants

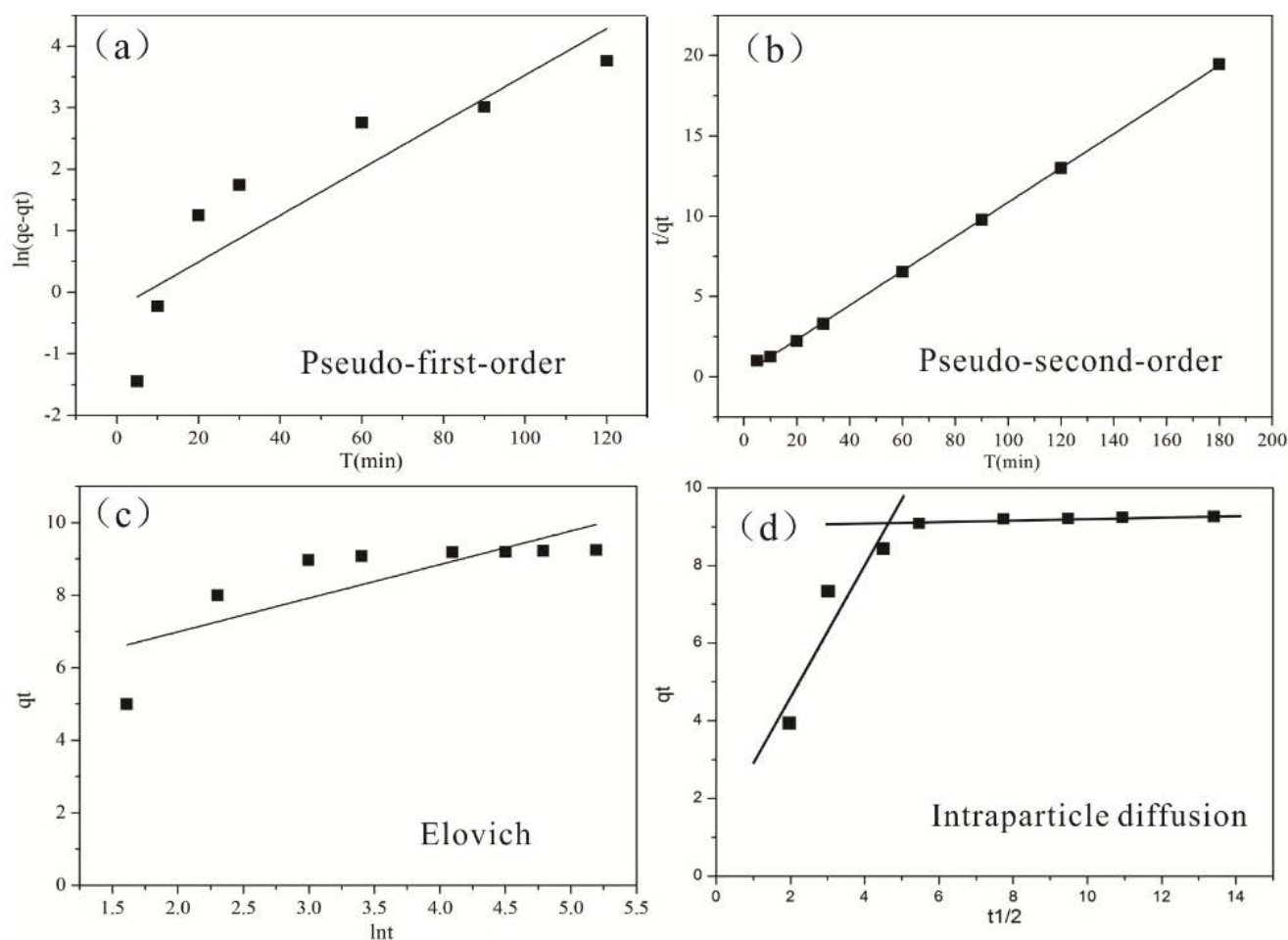| Pseudo-first-order		Pseudo-second-order		Intra-particle diffusion		Elovich	
q_e	0.7673	q_e	9.3756	C_{p1}	1.7142	α (mg g⁻¹ min⁻¹)	236.324
k_1 (mg g⁻¹ min⁻¹ᐟ²)	0.038	k_2 (mg g⁻¹ min⁻¹ᐟ²)	0.0557	k_{p1} (mg g⁻¹ min⁻¹ᐟ²)	1.7043	β (g⁻¹ mg)	1.078
r_1^2	0.7576	r_2^2	0.9996	r_{p1}^2	0.7153	r_3^2	0.5679
				C_{p2}	8.9944		
				k_{p2} (mg g⁻¹ min⁻¹ᐟ²)	0.0206		
				r_{p2}^2	0.8036		

Fig. 4. Fitted results of kinetic models: (a) pseudo-first-order, (b) pseudo-second-order, (c) Elovich, and (d) intra-particle diffusion.

The adsorption energy E (kJ mol^{-1}) is calculated from the D–R parameter K_{ad} as follows [17]:

$$E = -\left(2K_{ad}\right)^{-0.5} \tag{10}$$

The plot of the adsorption isotherms is shown in Fig. 5. The isotherm parameters are shown in Table 3. The E value is related to the physical and chemical adsorption [17]. The E value of the physical adsorption is less than 8 mol kJ^{-1}, whereas that of the chemical adsorption is greater than 8 mol kJ^{-1}. We found that the E value of this study was 15.110 mol kJ^{-1} (Table 1), demonstrating the Sb(III) ion adsorption onto the Fe-ATP beads tended to be chemical adsorption.

Table 3 shows that the experimental data fit the Freundlich model (0.9963) better than the Langmuir (0.9638) and Dubinin–Radushkevich models (0.9779), indicating that these sorbents had heterogeneous adsorption sites characterized by different Sb(III) ion adsorption energies. The Freundlich model is more adaptable to heterogeneous adsorption than multilayer adsorption [18]. The surface of the adsorbent was heterogeneous when n was within a range of from 1 to 10 [19]. As seen in Table 3, n was greater than 1, indicating that the adsorption of the Sb(III) ions onto the Fe-ATP beads was a heterogeneous adsorption process.

3.2.6. Thermodynamic studies

To research the adsorption thermodynamics of the Sb(III) ions onto the Fe-ATP beads, three basic constants, the change in $\Delta H°$ (kJ mol^{-1}), $\Delta G°$ (kJ mol^{-1}), and $\Delta S°$ (J mol^{-1} K^{-1}), were calculated using the following equations [26]:

$$\Delta G° = -RT \ln K_0 \tag{11}$$

$$\ln K_0 = \frac{\Delta S°}{R} - \frac{\Delta H°}{RT} \tag{12}$$

$$K_0 = \frac{a_s}{a_e} = \frac{\gamma_s q_e}{\gamma_e C_e} \tag{13}$$

where α_s and α_e are the activities of the adsorbed Sb(III) ions and the dissociative Sb(III) ions, respectively. γ_s is the activity coefficient of the Sb(III) ions and the dissociative Sb(III) ions, q_e is the Sb(III) ions adsorbed on the Fe-ATP beads (mmol g^{-1}), and C_e is the Sb(III) ion concentration in solution at equilibrium (mol L^{-1}).
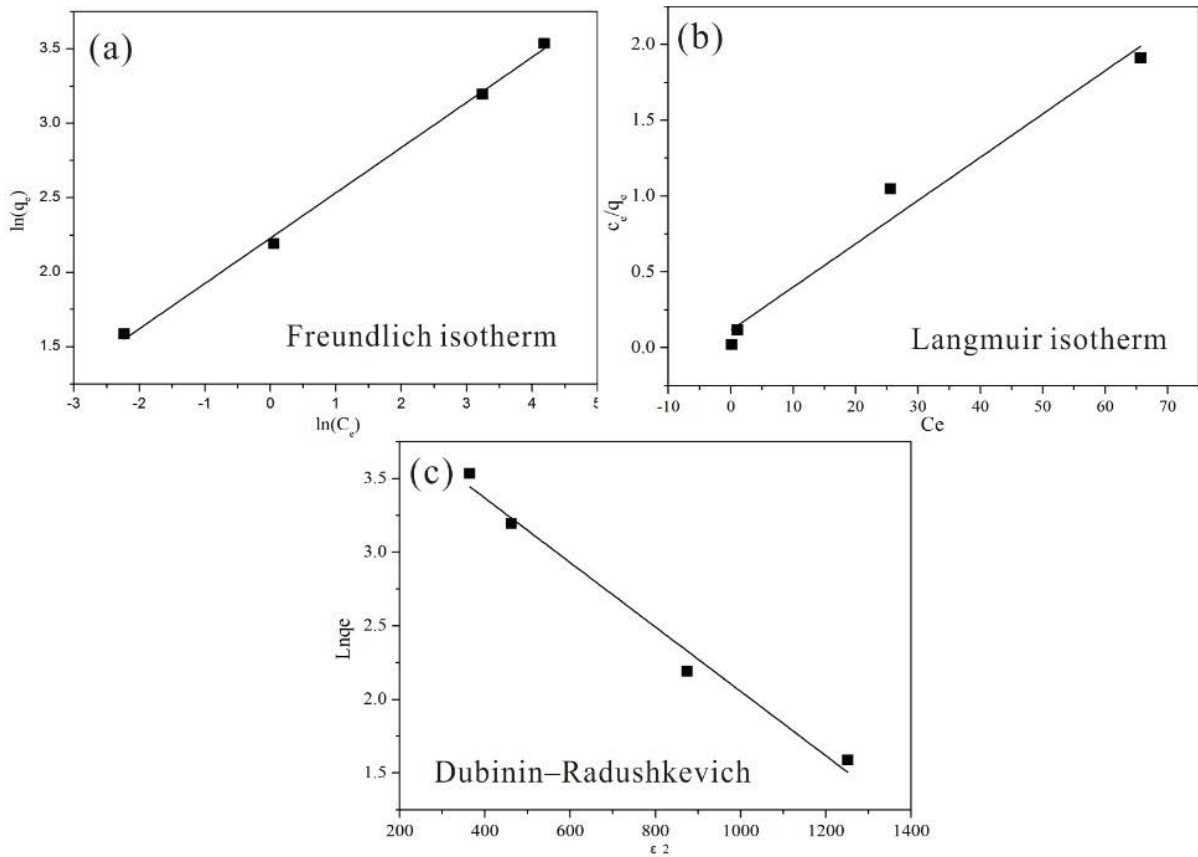
Fig. 5. Fitted model plots: (a) Freundlich isotherm, (b) Langmuir isotherm, and (c) Dubinin–Radushkevich.

Table 3
Fitted model parameters

Langmuir		Freundlich		Dubinin–Radushkevich	
q_m (mg g^{-1})	35.039	K_F	9.292	K_{ad} (mol^2 KJ^{-2})	0.00219
B (L mg^{-1})	0.248	n	3.290	q_s (mg g^{-1})	69.601
				E (mol kJ^{-1})	15.110
r_1^2	0.9638	r_2^2	0.9963	r_3^2	0.9779

K_0 can be calculated by $\ln(q_e/C_e)$ vs. q_e (Fig. 6a) and extrapolating to zero q_e. The values of $\Delta S°$ and $\Delta H°$ were calculated from the plot of K_0 vs. $1/T$. $\Delta G°$ was determined using Eq. (11). The adsorption constants of the Sb(III) ions on the Fe-ATP beads are listed in Table 4. The value of $\Delta G°$ for Sb(III) was negative, implying that the Sb(III) adsorption onto the Fe-ATP beads was spontaneous [22]. $\Delta H°$ was positive, indicating the adsorption was endothermic and it tended to occur at a higher temperature [23]. The positive
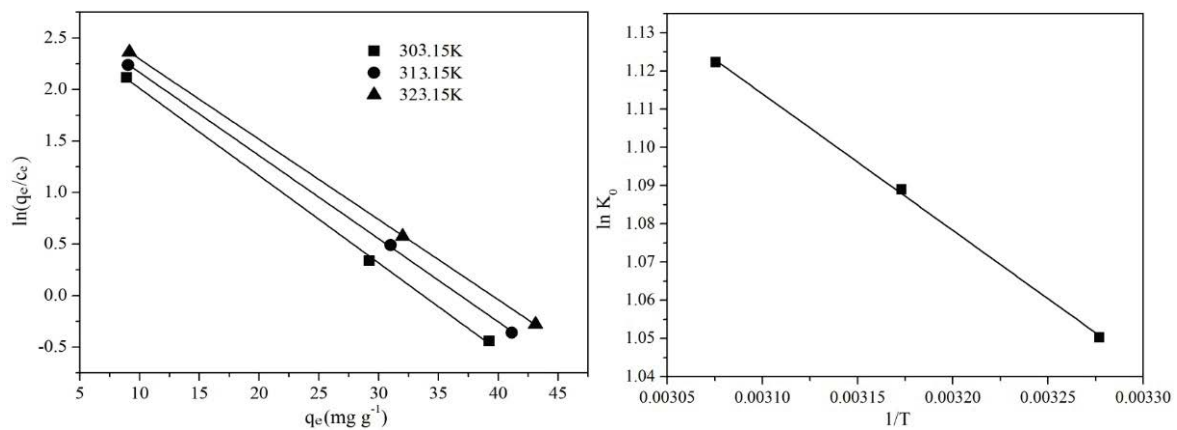

Fig. 6. Relevant parameters of the thermodynamics models.

Table 4
Thermodynamic model constants

Thermodynamic constants	Temperature (K)		
	303.15	313.15	323.15
K_0	2.8583	2.9713	3.0717
$\Delta G°$ (kJ mol^{-1})	−2.6668	−2.8558	−3.0364
$\Delta H°$ (kJ mol^{-1})	2.9733		
$\Delta S°$ (J mol^{-1} K^{-1})	18.4723		

Table 5
Sorption and desorption cycles using multi-component solutions

	Sorption efficiency (%)	Elution (%)
1st Cycle	92.8	85.4
2nd Cycle	91.5	86.9
3rd Cycle	90.1	88.07
4th Cycle	89.03	89.6
5th Cycle	87.2	90.3

value of $\Delta H°$ also could have been because of the occurrence of dissociative chemisorption [47,48].

3.2.7. Desorption

The reusability of the Fe-ATP beads was demonstrated by five sorption-desorption cycles. The results are shown in Table 5. The adsorption efficiency of Sb(III) tended to decrease, but it still remained greater than 80% after five cycles. The results showed that the Fe-ATP beads could be used in consecutive cycles.

The real wastewater was decontaminated by the Fe-ATP beads, and the concentration of Sb(III) ions decreased from 0.5 μg L^{-1} to below the detectable limit. The Fe-ATP bead is feasible to apply in real wastewater disposal.

4. Conclusion

The kinetics and isotherm for Sb(III) ion adsorption onto Fe-ATP beads could be well described using pseudo-second-order kinetics and the Freundlich isotherm, respectively. The sorption process was spontaneous and endothermic. The results showed that the synthesized Fe-ATP beads were good adsorbents for Sb(III) ion adsorption from an aqueous solution. The advantages of the Fe-ATP bead were that the adsorption efficiency remained high within a pH range of 1.0–11.0 and they had good adaptability to the solution pH. Moreover, the Fe-ATP beads had good regenerability and could be used in consecutive cycles. The Fe-ATP bead is a good adsorbent for Sb(III) ions in wastewater.

Acknowledgements

Symbols

b	—	Langmuir constant
C_0	—	Initial concentration of Sb(III)
C_e	—	Sb(III) ion concentration at equilibrium
C_{eq}	—	Sb(III) ion concentration in the solution at equilibrium
C_{pi}	—	Adsorption constant
C_t	—	Residual concentration of Sb(III)
k_1	—	First-order rate constant
k_2	—	Second-order rate constant,
K_f	—	Freundlich constant
k_{pi}	—	Rate constant for the intra-particle transport
m(g)	—	Mass of the adsorbents
q_0	—	Saturated monolayer adsorption capacity
q_e	—	Amount of Sb(III) ions at equilibrium
q_e	—	Sb(III) adsorption capacity at equilibrium
q_t	—	Amount of Sb(III) ions adsorbed at t time
T	—	Temperature (K)
V (L)	—	Volume of the adsorption system
α	—	Initial adsorption rate of the Elovich equation
α_s, α_e	—	Activities of the adsorbed Sb(III) ions and dissociative Sb(III) ions, respectively
β	—	Extent of the chemisorption surface coverage
γ_s	—	Activity coefficient of the Sb(III) ions and the dissociative Sb(III) ions

References

[1] J. Li, B. Zheng, Y. He, Y. Zhou, X. Chen, S. Ruan, Y. Yang, C. Dai, L. Tang, Antimony contamination, consequences and removal techniques: a review, Ecotoxicol. Environ. Saf., 156 (2018) 125–134.

[2] D. Amarasiriwardena, F. Wu, Antimony: emerging toxic contaminant in the environment, Microchem. J., 97 (2011) 1–3.

[3] C. Reimann, J. Matschullat, M. Birke, R. Salminen, Antimony in the environment: lessons from geochemical mapping, Appl. Geochem., 25 (2010) 175–198.

[4] X.L. Wu, D. Zhao, S.T. Yang, Impact of solution chemistry conditions on the sorption behavior of Cu(II) on Lin'an montmorillonite, Desalination, 269 (2011) 84–91.

[5] Y. Zhou, X. Liu, Y. Xiang, P. Wang, J. Zhang, F. Zhang, J. Wei, L. Luo, M. Lei and L. Tang, Modification of biochar derived from sawdust and its application in removal of tetracycline and copper from aqueous solution: Adsorption mechanism and modelling, Bioresour. Technol., 245 (2017) 266–273.

[6] T. Jiang, Y. Bao, W. Li, R.Y. Fang, H.X. Shi, Removal of antimony from water by nano zero-valent iron/activated carbon composites, Environ. Sci., 38 (2017) 4632–4640.

[7] Y. Cai, L. Li, H. Zhang, Kinetic modeling of pH-dependent antimony (V) sorption and transport in iron oxide-coated sand, Chemosphere, 138 (2015) 758–764.

[8] R.C. Vieira, S.C.R. Santos, R.A.R. Boaventura, H. Bacelo, M.S. Botelho, Recovery and valorization of tannins from a forest waste as an adsorbent for antimony uptake, J. Cleaner Prod., 198 (2018) 1324–1335.

[9] X. Yang, Z. Shi, M. Yuan, L. Liu, Adsorption of trivalent antimony from aqueous solution using graphene oxide: kinetic and thermodynamic studies, J. Chem. Eng. Data, 60 (2015) 806–813.

[10] F. Bullough, D.J. Weiss, W.E. Dubbin, J.C. Barry, J. Barrott, K.S. Arup, Evidence of competitive adsorption of Sb(III) and As(III) on activated alumina, Ind. Eng. Chem. Res., 49 (2010) 2521–2524.

[11] F. Arroyo-Torralvo, A. Rodríguez-Almansa, I. Ruiz, I. González, G. Ríos, C. Fernández-Pereira, L.F. Vilches-Arenas, Optimizing operating conditions in an ion-exchange column treatment applied to the removal of Sb and Bi impurities from an

electrolyte of a copper electro-refining plant, Hydrometallurgy, 171 (2017) 285–297.

[12] J.A. Allen, P.H. Scaife, The Elovich equation and chemisorption kinetics, Aust. J. Chem., 19 (1966) 2015–2023.

[13] M.M. Dubinin, L.V. Radushkevich, The equation of the characteristic curve of activated charcoal, Proc. Acad. Sci., Phys. Chem. Section., 55 (1947) 331.

[14] H.T. Fan, W. Sun, B. Jiang, Q.J. Wang, D.W. Li, C.C. Huang, K.J. Wang, Z.G. Zhang, W.X. Li, Adsorption of antimony(III) from aqueous solution by mercapto-functionalized silica-supported organic-inorganic hybrid sorbent: mechanism insights, Chem. Eng. J., 286 (2016) 128–138.

[15] L. Wang, C. Wan, D.J. Lee, J.H. Tay, X.F. Chen, X. Liu, Y. Zhang, Adsorption-desorption of strontium from waters using aerobic granules, J. Taiwan Inst. Chem. Eng.,44 (2013) 454–457.

[16] Y. Wang, Y. Feng, X.F. Zhang, X. Zhang, J. Jiang, J. Yao, Alginate-based attapulgite foams as efficient and recyclable adsorbents for the removal of heavy metals, J. Colloid Interface Sci., 514 (2018) 190–198.

[17] Z.J. Shao, X.L. Huang, F. Yang, W.F. Zhao, X.Z. Zhou, C.S. Zhao, Engineering sodium alginate-based cross-linked beads with high removal ability of toxic metal ions and cationic dyes, Carbohydr. Polym., 187 (2018) 85–93.

[18] L. Boudriche, R. Calvet, B. Hamdi, H. Balard, Surface properties evolution of attapulgite by IGC analysis as a function of thermal treatment, Colloids Surf., A, 399 (2012) 1–10.

[19] Z. Zhang, W. Wang, A. Wang, Highly effective removal of Methylene Blue using functionalized attapulgite via hydrothermal process, J. Environ. Sci., 33 (2015) 106–115.

[20] J. Xi, M. He, C. Lin, Adsorption of antimony(III) and antimony(V) on bentonite: Kinetics, thermodynamics and anion competition, Microchem. J., 97 (2011) 85–91.

[21] T.K. Naiya, A.K. Bhattacharya, S. Mandal, S.K. Das, The sorption of lead(II) ions on rice husk ash, J. Hazard. Mater., 163 (2009) 1254–1264.

[22] T. Kameda, M. Nakamura, T. Yoshioka, Removal of antimonate ions from an aqueous solution by anion exchange with magnesium-aluminum layered double hydroxide and the formation of a brandholzite-like structure., J. Environ. Sci. Health. Part A Toxic/Hazard. Subst. Environ. Eng., 47 (2012) 1146–1151.

[23] I. Langmuir, The constitution and fundamental properties of solids and liquids. Part I. Solids, J. Am. Chem. Soc., 38 (1916) 2221–2295.

[24] J.S. Markovski, D.D. Marković, V.R. Dokić, M. Mitrić, M.D. Ristić, A.E. Onjia, A.D. Marinković, Arsenate adsorption on waste eggshell modified by goethite, α-MnO$_2$ and goethite/α-MnO$_2$, Chem. Eng. J., 237 (2014) 430–442.

[25] S. Mishra, N. Sankararamakrishnan, Characterization, evaluation, and mechanistic insights on the adsorption of antimonite using functionalized carbon nanotubes, 25 (2018) 12686–12701.

[26] A. Sari, D. Çitak, M. Tuzen, Equilibrium, thermodynamic and kinetic studies on adsorption of Sb(III) from aqueous solution using low-cost natural diatomite, Chem. Eng. J., 162 (2010) 521–527.

[27] H. Freundlich, Über Die Adsorption in Lösungen, Engelmann, Leipzig, 1906.

[28] M.V. Subbaiah, G. Yuvaraja, Y. Vijaya, A. Krishnaiah, Equilibrium, kinetic, and thermodynamic studies on biosorption of Pb(II) and Cd(II) from aqueous solution by fungus (Trametes versicolor) biomass, J. Taiwan Inst. Chem. Eng., 42 (2011) 965–971.

[29] X.Y. Zhou, X. Zhou, The unit problem in the thermodynamic calculation of adsorption using the Langmuir equation, Chem. Eng. Commun., 201 (2014) 1459–1467.